Part II

Theoretical

2

Bubble Nucleation

2.1 Introduction

In this chapter we investigate theoretically the use of an ultrasound pulse to generate submicron bubbles. Submicron bubbles are important because they resonate at higher-frequencies, enabling imaging at higher resolutions; and because they are more likely to leave the blood than conventional micron-sized bubbles, the crucial first step towards functional diagnostic contrast imaging.

Broadly, there are two approaches to acoustically generating a bubble:

1. produce a bubble from the bulk fluid directly. In medical ultrasound the bulk will invariably be some aqueous solution.
2. introduce a second fluid, immiscible to the bulk, from which to generate bubbles. This second fluid - an oil in the aqueous bulk - can be chosen with properties to facilitate the acoustic generation of a bubble.

Unfortunately, this division in methodology does not make clear the mechanisms by which a bubble may be generated. The bulk fluid will, unless extraordinary efforts are undertaken, contain small particles of dust that may or may not entrap pockets of gas, contain gas bubbles stabilised with trace amounts of detergent, in addition to containing a host of dissolved gases. Likewise for any secondary fluid that is introduced, with the additional complication of the water-oil interface becoming a rest point for other impurities in the system and developing a complex chemistry of its own. Bubble generation is extremely sensitive to the surface chemistry of a nascent bubble [104], while the presents of motes and existing bubbles can change the mechanism of bubble generation entirely. The presence of dissolved gasses is also known to be important in bubble generation [107], although this case is not investigated in this thesis.

Historically the term *cavitation* has been used ambiguously with respect to the mechanism of bubble formation. It is therefore helpful to instead use the word *nucleation* with the more careful categorisation of Jones [49]:

Type 1: classical homogeneous nucleation: a bubble is *created* within the bulk medium where no bubbles were present prior to the reduction in pressure,

Type 2: classical heterogeneous nucleation: a bubble is *created* upon a solid particle floating in the medium, or in a crevice in the surface of the container,

Type 3: pseudo classical nucleation: a bubble results from a *pre-existing* but sub-critical gas cavity. The gas cavities may be stabilised by a crevice in a floating particle or by a crevice in the container, or may be bubbles stabilised by a variably permeable skin [121]. Sub-critical means that their curvature is smaller than the *critical radius*, the radius at which the bubble is in equilibrium with its surroundings. The bubble must still overcome an energy barrier to grow.

Type 4: non-classical nucleation: a bubble results from a *pre-existing* gas cavity but there is no energy barrier to growth. This occurs when the radius of curvature of a crevice is larger than the critical radius. It is the lack of the energy barrier that makes this nucleation non-classical.

With these differing mechanisms in mind our two broad methodologies are revisited. By what mechanism can the bulk fluid (water) be nucleated with ultrasound? Is the mechanism the same in an oil emulsion?

2.1.1 The nucleation of water

The pressures required for water to undergo type I nucleation are prohibitive for diagnostic ultrasound. Herbert [37] measured the nucleation probability to be vanishingly small at -20 MPa, with the probability rising to 50% at -26 MPa, a result typical of other measurements [36]. However, gas can be extracted from water at negative pressures at a few atmospheres [116]. Such nucleation events must result from another mechanism.

Motes promote nucleation by reducing the surface area of the vapour-liquid interface, thereby reducing the energy required to form the bubble. In the absence of entrapped gas - when the crevices are fully *wetted* with the bulk fluid - type 2 nucleation occurs. The reduction in the energy barrier can be considerable and is greatest when the crevices are deep and narrow [66]. Herbert [37], for instance, noted that while tap water has the same 50% cavitation threshold as purified water, tap water has a very long tail of rarer nucleation events at much less extreme pressures. Although not fully determined in the article, it seems reasonable to suggest that these events occur through type II nucleation: Herbert uses repeated pulses that have negative pressures in excess of 15 MPa and at such high pressures it is likely that gas entrapped in motes is removed by earlier pulses. This would be consistent with a 50% cavitation threshold that is identical to purified and degassed water, a result that is hard to reconcile if there is entrapped gas within the system.

Nucleation events in human tissue are relatively rare, and do not become probable until the type I/II nucleation thresholds of water [113]. Biology, it seems, is very adept at preventing gas pockets from occurring within tissue.

The high cavitation pressures recorded for type I and type II nucleation mean that the nucleation of impure water at diagnostic pressures is believed to pro-

ceed via type III and IV nucleation [5;12;49]. There are two models for type III and IV nucleation. The first is that partially wetted motes trap gas [5] and the second is that organic impurities stabilise freely floating gas bubbles [121]. Both suggestions have been observed experimentally [12;48] and both are thought to be important in practice.

Due to the high cavitation pressures in biological tissues, a medium that introduces Type III and IV nucleation events is a prime targets for developing a contrast agent. These media have traditionally introduced stabalised micron sized bubbles. There is no reason why they should not, alternatively, introduce gas entrapped in motes, such as are found in regular tap water.

2.1.2 The nucleation of an oil droplet within an emulsion

To leave the blood through leaky tumour vasculature the radius of a droplet must be at most 300 nm [30;35;40]. What is the likely nucleation mechanism for a droplet this small? Let us first estimate the probability that the droplet contains a mote.

The probability that a droplet contains a mote depends both on the purity of the oil used to make up the droplets and the purity of the surrounding medium. We assume that the proportion of oil in the medium is small and that the impurities from the bulk dominate. We also neglect any differences in the affinities of the oil and bulk to the mote. Finally, we suppose that we make no special effort to either clean or dirty the water, but instead take the water straight from the tap. For the mote-density of tap water we shall use Apfel's [4] suggestion of 10^5 cm^{-3}.

From Apfel's density it follows that for every mote there will be

$$\frac{1}{\text{motes per volume} \times \text{volume per droplet}} = 10^8 \tag{2.1}$$

droplets with a radius of 300 nm. Since a pre-existing gas bubble (stabalised or not) would have to be exceptionally small to be trapped within 300 nm oil droplet, we conclude that the oil droplets of interest are likely to undergo type I nucleation. Indeed, the use of small droplets to avoid the problems of 'dirty' water is a well used technique for experimentally investigating type I nucleation [4;79;112]. For instance, Turnbull [112] found that droplets of 2-8 µm bubble are required to homogeneously freeze mercury. Such droplets are already an order of magnitude larger than what is required to leave the blood, and it therefore seems reasonable to suggest that smaller droplets will nucleate homogeneously.

Type I nucleation can be challenging to initiate. For an oil to undergo type I nucleation at conventional ultrasound pressures it must either have a much lower boiling point than water, or be able to dissolve a much greater concentration of gas. In this chapter we consider the perfluorocarbons. This series of oils is characterised by their low boiling points, given in Table 2.1, and their high solubility of many gases. The perfluorocarbons are also chemically inert and have been used before in medical applications [57;92].

Table 2.1: Boiling points and critical temperatures of various perfluorocarbons

	Boiling Point (°C)	Critical Point (°C)
Perfluoroethane	-78	20
Perfluoropropane	-38	72
Perfluorobutane	-1.7	113
Perfluoropentane	29	149
Perfluorohexane	59	176

To simplify the discussion further, this chapter assumes that the type 1 nucleation occurs entirely within the perfluorocarbon droplet. The water is neglected. The exceptionally low solubility (a few parts per million[115]) of the perfluorocarbons in water goes some way to justify this approximation.

The assumption is not without its problems. The small size, potentially, could make a droplet a poor approximation to an 'infinite thermodynamic system', with the finite volume errors that this can entail. However, neglecting the nucleation at the interface remains a limitation of our approach. Techniques for lifting the restriction have been considered by others[45;50], but we do not pursue these here.

2.1.3 Structure of the chapter

During the course of this thesis two contrast media with two differing nucleation mechanisms shall be investigated: the type III/type IV nucleation of a mote found in "dirty water", and the type I nucleation of an oil droplet. In the first case the driving wave is used to evacuate gas entrapped on motes and to manipulate the size of the resulting (and pre-existing) bubbles. In the second case the driving wave is used to initiate the nucleation of the perfluorocarbon droplet and manipulate the resulting bubble's diameter.

Three preliminary questions need to be addressed in order to investigate the role of the driving wave in each of these mechanisms:

1. What size of bubble will be generated from each nucleation mechanism?
2. What pressures are required to generate type I nucleation of bubbles?
3. What is the lifetime of the generated bubbles? Is there time for them to be imaged with ultrasound before they redissolve into the fluid?

Each of these questions depend upon the *critical radius* of a bubble - the radius at which it is thermodynamically favourable for the bubble to neither grow nor shrink. In the first case, the critical radius must be reached for a bubble to grow beyond its nascent state, or to free itself rather than shrink back into its crevice. The critical radius therefore provides, as a function of pressure, a

lower bound to the size of the bubble. Secondly, the critical radius defines the energy required for the bubble to form. The probability of a type I nucleation event then follows via the Aarenhius equation. Finally, the critical radius is a limiting radius when calculating the lifetime of a generated bubble.

The evaluation of the critical radius is therefore the first objective of this chapter. It will be discussed in detail in section 2.2 and will directly answer the first of our questions. The pressures required for type I nucleation will be calculated in section 2.4. Finally, the lifetimes of the expected bubbles will be calculated in section 2.5.

2.2 The critical radius of a bubble

2.2.1 The definition of the critical radius

When the rarefactional pressure of the acoustic wave exceeds the atmospheric pressure it places the fluid under tension. The creation of a vapour bubble relaxes this pressure but also creates an interface. Creating a small bubble is energetically unfavourable because the energy required to maintain the interface dominates. A large bubble, on the other hand, will grow explosively when placed under tension because the relaxation in pressure caused by the bubble's volume dominates. For a given pressure there exists, therefore, a *critical radius*, a^*, at which the bubble neither grows nor shrinks but is at thermodynamic equilibrium. If spherical symmetry is assumed then the critical radius is such that [77;78]

$$\frac{d\Omega}{da} = 0, \quad \text{at } a = a^* \tag{2.2}$$

where Ω is the *grand potential* and a is the bubble's radius.

2.2.2 The capillary approximation to the critical radius

The grand potential is straight forward to evaluate if it is assumed that:

- the density of the liquid,
- the equilibrium vapour pressure and
- the equilibrium surface tension between liquid and vapour

all take their bulk values. This set of assumptions is the capillary approximation: the liquid and bubble are assumed to be separated by a sharp interface and the surface tension is taken to be that of the macroscopic plainer interface. The argument strictly applies only in the thermodynamic limit.

When the nucleating bubble is very small the thermodynamic limit can be a poor approximation [105]. The distance over which the density changes from liquid to vapour if often not insignificant and the surface tension is typically

reduced from its bulk value [54]. We shall investigate the validity of the capillary approximation for the case of water and perfluoropentane in section 2.6.2, but for the time being we continue.

If a bubble is created adiabatically then the energy required to form a bubble of radius a is [16;51]

$$\Delta\Omega = 4\pi\gamma a^2 - \frac{4\pi a^3}{3}\left(p_v - p_L\right) + i\left(\mu_v(p_v) - \mu_L(p_L)\right). \tag{2.3}$$

Here $\Delta\Omega$ is the change in the grand potential, γ is the surface tension. p_L and p_v are the pressures of the oil droplet and the vapour, $\mu_L(p_L)$ and $\mu_v(p_v)$ are the chemical potentials (per molecule) of the oil droplet and vapour at their given pressures, and i is the number of molecules in the newly created vapour bubble. The first term on the right hand side of equation 2.3 is the contribution from the surface tension. The second is the energy released by the change in volume, the third is the energy generated from the chemical potential by the transport of molecules.

The critical radius is when the energy barrier $\Delta\Omega$ is minimal (equation 2.2). By differentiating 2.3 with respect to a it is found to be

$$a^* = \frac{2\gamma}{p_v^* - p_L}, \tag{2.4}$$

which is the Laplace relation. The pressure, p_v^*, is the critical pressure within the bubble. Due to the bubble's curvature it is not equal to the equilibrium vapour pressure of a flat interface, denoted p_∞. The two vapour pressures are related by the Poynting correction,

$$p_v^* = p_\infty \exp\left(\frac{V_m\left(p_L - p_\infty\right)}{RT}\right), \tag{2.5}$$

where V_m is the molar volume and R is the ideal gas constant. Equation 2.5 is derived, for completeness, in Appendix B.

Substituting 2.4 into 2.3 gives the energy required to create a bubble of critical radius,

$$\Delta\Omega^* \equiv \Delta G|_{a=a^*} = \frac{16\pi\gamma^3}{3\left(p_v^* - p_L\right)^2}. \tag{2.6}$$

The chemical potentials have vanished from 2.6 because the bubble is at thermodynamic equilibrium, whence the Grand Potential equates to the Free Energy, G, because

$$\mu_v(p_v^*) = \mu_L(p_L), \quad \text{at } a = a^*. \tag{2.7}$$

2.3 Question 1: A lower bound on the size of a bubble

We are now in a position to answer the first of our questions: the size of bubble expected to be cavitated. This is because the critical radius provides a

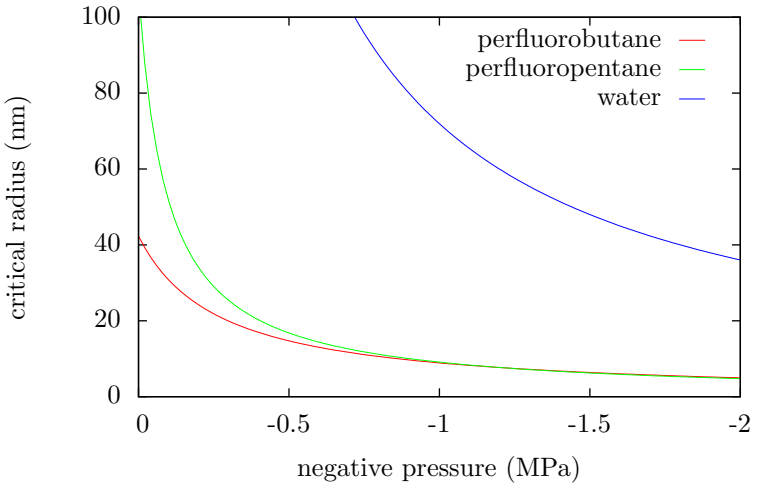

(a)

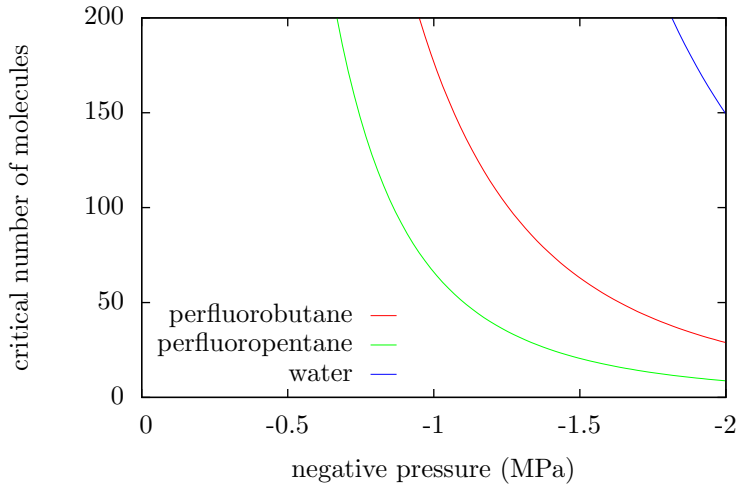

(b)

Figure 2.1: Capillary predictions for the critical radius and critical number of molecules for a bubble as a function of the pressure at 298 K. The vapour is assumed to be an ideal gas, with the vapour pressure obtained by experimental fits to Antoine's equation. The coefficients for Antoine's equation are taken from National Institute of Standards Database[64] (Note that the perfluorobutane data is used outside of its range of validity, see text).

lower bound for vapour bubbles in solution. A bubble smaller than the critical radius will shrink even when placed under tension, and so is very unlikely to be observed.

Figure 2.1a uses equation 2.4 to plot the the critical radius as a function of pressure for water, perfluoropentane and perfluorobutane at 298 K. The capillary approximation predicts that the critical radius is smaller for the perfluorocarbons than for water. This is encouraging, for it implies that type I nucleation is easier to induce for the perfluorocarbons than for water.

At high pressures the critical radii of the two perfluorocarbons converge. This is because the critical radius depends linearly on the surface tension (equation 2.4) and the surface tensions are similar for perfluorocarbons. Using a perfluorocarbon with a lower boiling point will enable smaller stable bubbles only at the more moderate pressures where the vapour pressure plays a greater role. If higher pressures are used then the effect is negated.

It should be noted that the vapour pressure used for perfluorobutane was extrapolated by 29 °C outside of its range of validity[64] by use of Antoine's equation. Since 25 °C is above the boiling point of perfluorobutane no equilibrium vapour pressure can be defined. However, since 25 °C is also well below the critical temperature, it is hoped that the predicted pressures within the (super-heated) bubble are still meaningful.

In Figure 2.1b the predicted number of molecules contained within a critical bubble are plotted. Again and as expected the number of perfluorocarbon molecules required to form a bubble are smaller than for water. Figure 2.1b does, however, illustrate the difficulty with the capillary approximation being used. It is highly questionable that a bubble containing tens or even hundreds of molecules behaves like its thermodynamic bulk, with a constant density until the interface.

The capillary approximation predicts that a greater number of molecules are required to form a critical bubble for perfluorobutane than for perfluoropentane. This is again due to the higher vapour pressure of perfluorobutane.

2.4 Question 2: The vapourisation pressure of a perfluorocarbon droplet

There are two possible goals that may be set when imaging a bubble generated from a perfluorocarbon droplet:

1. image the actual vaporisation event,
2. image the resultant bubble after it has vaporised but before it redissolves.

Due to the stochastic nature of bubble nucleation, the pressures required to achieve these goals are best expressed in terms of pressures required to achieve a given rate of nucleation, the rate being such that observations are likely in the time frame of a given experiment.

2.4.1 The rate required to image a vaporisation event

For a nucleation event to be directly imaged it must occur within the acoustical volume of the imaging pulse - the volume in which the pressure is near its peak. The imaging volume is most simply approximated as a cylinder and the pulse's principle wavelength, λ, makes a reasonable estimate for the diameter of a focused pulse. If the pulse is n cycles long then the acoustical volume, V, is given as so,

$$V \approx \frac{n\pi\lambda^3}{4}. \tag{2.8}$$

The duration of the pulse is $\tau_p = n\lambda/c$ and so it follows that the rate, R, at which the medium is sampled is

$$R \approx V/\tau_p = \frac{c\pi\lambda^2}{4} \tag{2.9}$$

The sampling rate of a 15 MHz imaging pulse is therefore approximately 10 $\mathrm{cm}^{-3}\mathrm{s}^{-1}$. This gives the minimal rate of nucleation that would be expected to be observed with a single a-line pulse. It is only marginally greater than the limit of observation typically chosen in other nucleation applications: 1 $\mathrm{cm}^{-3}\mathrm{s}^{-1}$ [79]. For consistency with other applications, we therefore use this latter definition of 1 $\mathrm{cm}^{-3}\mathrm{s}^{-1}$ as the limit of what can be observed with ultrasound. This corresponds to one nucleation event every 10 pulses.

2.4.2 The rate required to image a generated bubble

If only the bubble resulting from a nucleation event needs to be imaged, rather than the nucleation event itself, then the observable rate of nucleation is much lower. This is because the bubble is potentially observable if the pulse passes within its lifetime and so it is the lifetime of the bubble, τ_b, and not the duration of the acoustical pulse, that defines the observable nucleation rate,

$$R \approx V/\tau_b = \frac{n\pi\lambda^3}{4\tau_b} \tag{2.10}$$

The value of τ_b will be evaluated when we consider the third of our questions in section 2.5.

2.4.3 The rate of bubble nucleation

The rate of nucleation per unit volume is given by the Aarenhius equation,

$$J = J_0 \exp\left(-\frac{\Delta\Omega}{k_B T}\right), \tag{2.11}$$

where $\Delta\Omega$ is the energy barrier to nucleation (in terms of the Grand Potential, Ω), k_B is Boltzmann's constant, T is the temperature and J_0 is a rate (per unit

Table 2.2: Dimensionless groups in the calculation of the nucleation rate constant

	Parameter	Symbol	Dimension
Bubble	Rate of bubble growth	J_0	$[L]^3[t]^{-1}$
	Vapour number density	ρ_v	$[M][L]^{-3}$
	Surface tension	γ	$[M][T]^{-2}$
Fluid	Fluid number density	ρ_l	$[M][L]^{-3}$
Particle	Particle mass	m	$[M]$

volume) obtained when $T \to \infty$ or when $\Delta\Omega \to 0$.

The rate constant, J_0, for bubble nucleation is problematic. The reason is that the definition of a very small bubble is not clear conceptually. What is meant, for example, by a bubble of three molecules? And how does one know when a new molecule has joined it? Such uncertainties mean that arguments for J_0 very rapidly lose their precision. In contradistinction, the formation of a liquid droplet from a saturated vapour is clear conceptually: a droplet of three molecules is easy to envisage, a cluster of just a few molecules is easier to define than a void. Collision theory provides plausible arguments for the rate of droplet formation in a saturated vapour [51]. Be it on the grounds of reciprocity, or simply because a better alternative cannot be found, the rate constant J_o for bubble formation is usually taken to be the same as that for the formation of a liquid droplet from a saturated vapour [76].

Rather than repeat a spurious argument we prefer to estimate J_0 by dimensional analysis. The result is the same as that used in the literature and is obtained at a fraction of the effort. In addition, the estimate obtained here does not give the impression of greater accuracy than it deserves, a danger ever present in kinematic derivations.

At high temperatures, or when the energy barrier ΔG vanishes, one would expect the detailed chemistry of the medium to become unimportant with the liquid medium characterised as a collection of point particles of mass, m, and number density, ρ_l. Likewise, a vapour bubble within the medium characterised by its number density, ρ_v, and surface tension, γ. These properties are summarised in Table 2.2 along with their dimensions. There are five variables listed comprising of three dimensions: mass $[M]$, length $[L]$ and time $[t]$. It is therefore possible to write down 2 dimensionless groups [33].

To eliminate the temporal dependence J_0 must be squared and combined with surface tension. The resulting J^2/γ has the units $[M]^{-1}[L]^{-6}$. These dimensions can be cancelled by using the particle mass and the square of a number density. There is a choice as to which of the number densities, ρ_L and ρ_v, should be used. Le Chatelier's principle advices that that denser liquids are more expensive (in terms of energy) to separate, and that denser bubbles are less expensive to maintain. One would expect, therefore, the rate J_0 to be

proportional to ρ_v.

$$\Pi_1 = \frac{J_0^2 m}{\gamma \rho_v^2}. \tag{2.12}$$

The second dimensionless group that can then be formed is then simply ratio of the densities,

$$\Pi_2 = \frac{\rho_v}{\rho_L}. \tag{2.13}$$

Writing Π_1 as some function, g, of Π_2 we obtain,

$$J_0 = \rho_v \sqrt{\frac{\gamma}{m}} g\left(\frac{\rho_v}{\rho_L}\right). \tag{2.14}$$

The function g is undetermined but for the reasons just argued we anticipate g to increase with ρ_v and decrease with ρ_L. The simplest such relationship is a linear one and so we guess $g(x) \propto x$. If the constant of proportionality is assumed to be approximately unity, then for bubble nucleation we have

$$J_0 \approx \frac{\rho_v^2}{\rho_l} \sqrt{\frac{\gamma}{m}}, \tag{2.15}$$

This is identical to the result of the collision theory argument of Katz [50]. For water $J_0 \approx 10^{34}\text{cm}^{-3}\text{s}^{-1}$ and for perfluoropentane $J_0 \approx 10^{32}\text{cm}^{-3}\text{s}^{-1}$.

2.4.4 Results

The nucleation rates calculated with the capillary approximation are plotted in Figure 2.2. In Figure 2.2a the rates for perfluorobutane, perfluoropentane and water are plotted. As expected from the plot of critical radii, Figure 2.1a, high rates of nucleation are obtained at lower pressures with the perflurocarbons than for water, with perfluorobutane being more easily cavitated than perfluoropentane. This is encouraging, for increasing the rate of type I nucleation was the motivation for considering the perfluorocarbons.

However, the pressures given by Figure 2.2 to observe type I nucleation are high for diagnostic ultrasound. Figure 2.2a suggests that perfluorobutane, even when in a supersaturated state, will require a negative pressure in the region of 4 MPa to be observable. Such pressures are used in medical ultrasound, but require the specially engineered transducers of HIFU. To observe perfluoropentane the negative pressure will need to be in the region of 8 MPa, and while Figure 2.2b shows that the temperature is influential, it is not so influential as to shift the pressures back to those obtainable with diagnostic transducers. These pressures are of the same order of magnitude as the experimental values of Schad [94].

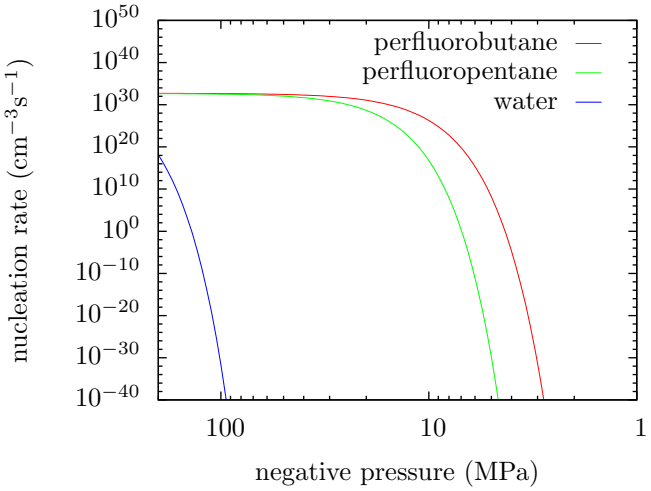

(a) Nucleation rates for water, perfluoropentane and perfluorobutane at 25°C.

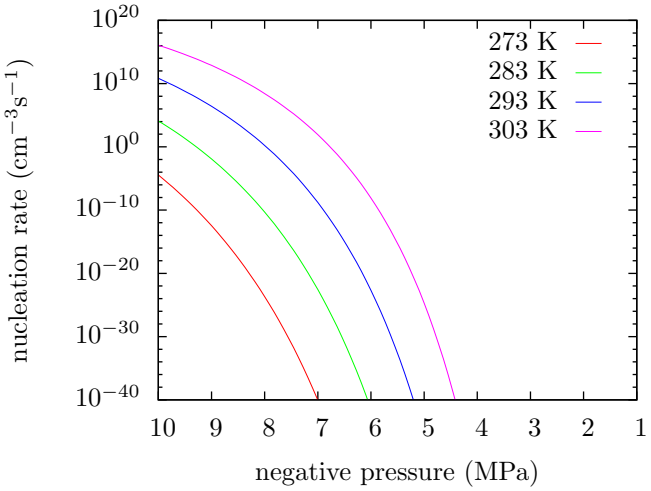

(b) Nucleation rates for perfluoropentane at different temperatures.

Figure 2.2: Nucleation rates evaluated from equation 2.11. The NIST Chemistry WebBook[64] being used as the source for the required experimental constants.

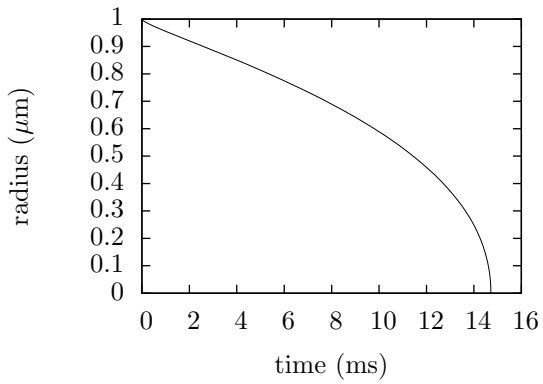

(a) Dissolution of a 1 µm air bubble when $\zeta = 0$

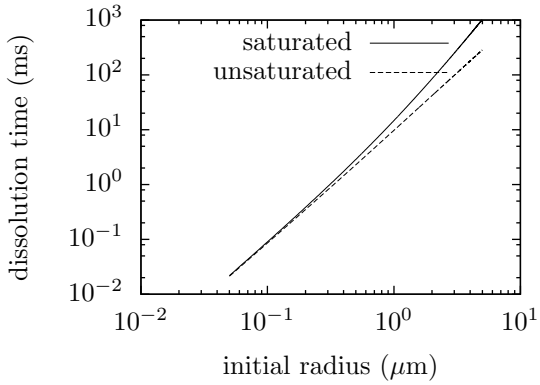

(b) Dissolution time as a function of radius

Figure 2.3: Dissolve times of air bubbles. The experimental quantities used in the model are given in Table 2.3.

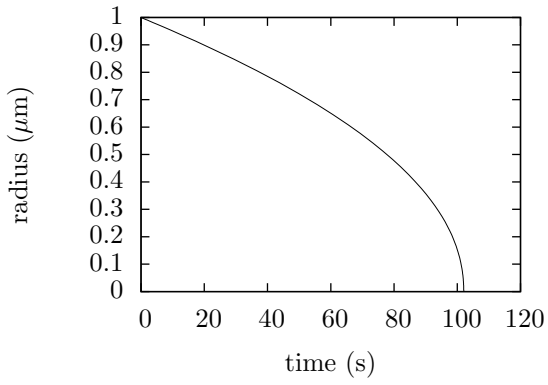

(a) Dissolution of a 1 µm perfluoropentane bubble when $\zeta = 0$

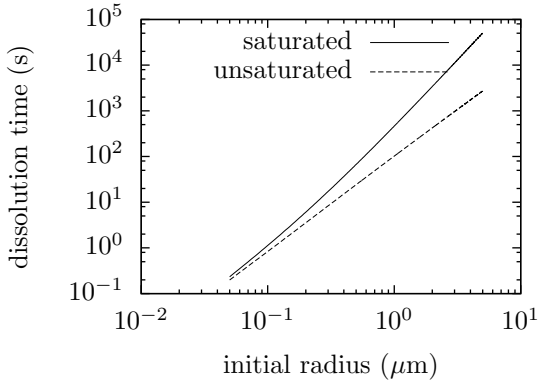

(b) Dissolution time as a function of radius

Figure 2.4: Dissolve times of perfluoropentane bubbles. The experimental quantities used in the model are given in Table 2.3.

2.5 Question 3: The lifetime of a vapour bubble

The third and final question of this chapter regards the expected lifetime of a bubble. In section 2.3 the critical radius was used to give a lower bound on the size of a bubble generated in a perfluorocarbon droplet or evacuated from a moat. It was seen that bubbles in the tens of nanometres can be stable when placed under tension by the rarefactional cycles of an acoustic field. The expected lifetime of the bubble after the rarefaction has passed will now be calculated.

This section uses a very simple model that was first derived by Epstein and

Table 2.3: Symbols used in the calculation of dissolution times

Symbol	Description	units	Value (Air)	Value (PFP)
γ	Surface tension	N/m	0.07280 [93]	0.0096828 [64]
H	Henry's constant	$m^2kgs^{-2}mol^{-1}$	1.48472×10^{-7} [93]	3.54634×10^{-4} [103]
D	Diffusivity	m^2s^{-1}	2.05×10^{-9} [93]	6.409×10^{-10} [a]
P_∞	Ambient Pressure	MPa	0.101325	0.101325

[a] Estimated with the Hayduk-Laudie equation

Plesset [21], although we prefer the notation of Gor [34]. The hope is to obtain only an order of magnitude estimate of the bubble lifetime and so some accuracy can be foregone.

In the model a gas bubble is placed in a fluid of uniform pressure, where the medium in the vacinity of the bubble contains the gas at concentration n_o. Two gas bubbles will be considered, an air bubble that contains nitrogen and oxygen, and a perfluoropentane bubble. In each case it will be assumed that the bubble contains no water vapour, and that the surface of the bubble is has no stabailising shell[1]. The concentration of the medium far from the bubble is denoted n_∞ and is chosen to be the ambient density of the gas in the medium at standard temperature, T, and pressure, p_∞. While we imagine the bubble to be generated in a rarefaction cycle of an acoustic wave we neither model the generation of the bubble nor the sound pulse.

There are two cases of particular interest

1. when the concentration of dissolved gas in the bubble's vacinity is equal to the ambient concentration,

$$n_0 = n_\infty. \tag{2.16}$$

   Such will be the case when a bubble in generated in a medium that is unaltered by the passing of the acoustic wave. This will typically be the case for short pulses of low pressure.

2. when the concentration of the gas in the bubble's vacinity is much lower than the ambient concentration. This situation can arise when a previous pulse of a high pressure wave has already evacuated most of the gas in the focal zone. The limiting case is when

$$n_0 = 0. \tag{2.17}$$

It is therefore natural to frame the derivation in terms a dimensionless measure of saturation,

$$\zeta \equiv \frac{n_0 - n_\infty}{n_\infty} \tag{2.18}$$

[1] See Sarkar [93] for a recent discussion of the dissolation of a bubble that has a permeable shell.

The two cases of interest are when $\zeta = 0$ and $\zeta = -1$. The solubility of the medium will make a second useful dimensionless quantity [34]

$$s \equiv \frac{k_B T n_\infty}{P_\infty}. \tag{2.19}$$

Imbalances in the number density of the gas in the medium will prompt diffusion from the vacinity of the bubble to the bulk. Modelling this as Fickian diffusion in a spherical geometry gives,

$$j_D = -D\frac{\partial n}{\partial r} \tag{2.20}$$

where the density is a spherical symmetric function of radius, r. If diffusion transport terms are neglected then 2.20 can be solved to obtain,

$$\frac{\partial n}{\partial r} = (n_R - n_0)\left[\frac{1}{R} + \frac{1}{\sqrt{\pi D t}}\right], \tag{2.21}$$

where R is the bubble radius and n_R is the concentration of dissolved gas at that radius. The details of the derivation were given in Epstein and Plesset's [21] original paper and do not need to be reproduced here.

Material conservation requires that the number of particles passing through the radius of the bubble equates to the change in the number of particles in the bubble, N,

$$\frac{dN}{dt} = 4\pi R^2 j_D \frac{\partial n}{\partial r}. \tag{2.22}$$

Modelling the contents of the bubble as an ideal gas lets the particle number be expressed in terms of the ambient pressure, P_∞, and surface tension γ of the bubble,

$$N = \frac{4\pi R^3}{3k_B T}\left[P_\infty + \frac{2\gamma}{R}\right]. \tag{2.23}$$

By differentiating 2.23 and equating the result to 2.22 a differential equation for the change in bubble radius is obtained,

$$\dot{R}\left[1 + \frac{4\gamma}{P_\infty R}\right] = Ds\left[\zeta - \frac{2\gamma}{P_\infty R}\right]\left[\frac{1}{R} + \frac{1}{\sqrt{\pi D t}}\right], \tag{2.24}$$

where equation 2.19 has been used, along with

$$\frac{(n_0 - n_R)}{n_\infty} = \zeta - \frac{2\gamma}{P_\infty R} \tag{2.25}$$

which follows from 2.18.

The numerical solution of 2.25 is plotted for a 1 micron air bubble in Figure 2.4. It is seen that the bubble radius decreases fairly constantly until a very rapid final callapse. The lack of a long tail in Figure 2.4 means that the dissolution

time is dominated by periods when the bubble is near is starting radius. There is not a long decay during which the bubble is technically existent but is so small as to be unobservable.

The dissolution time for an air bubble as a function of radius is plotted in Figure 2.3b. Both the saturated and unsaturated cases are plotted. The dissolution times for very small bubbles is very similar, but starts to diverge for bubbles of radius 0.5 µm.

The lifetime of a free submicron air bubble is of order 1 ms in both the saturated and unsaturated cases. The pulse duration of diagnostic ultrasound is typically measured in microseconds and so the bubble would be expected to live throughout the duration of the pulse. However, adjacent alines in a diangostic pulse are often tens of milliseconds apart. Submicron air bubbles would not be expected to exist in adjacent alines. The short lifetimes of air bubbles mean that care needs to be taken to syncronise the generation and the imaging of a bubble, so that the imaging wave samples the same focal region as the driving wave within a few microseconds of the driving wave passing.

The solubility of the perfluorocarbons in water is much lower than for nitrogen and oxygen. While the dissolution characteristics are very similar to an air bubble (Figure 2.4b) the timescale for dissolution is order of magnitudes larger (Figure 2.4a). This has the advantage that a bubble can be generated at a different time (and therefore at a different location) to where the bubble is imaged. In this case the driving wave and the imaging wave can be considered independently.

2.6 Discussion

2.6.1 Summary of results

In this chapter the two broad approaches of generating a bubble with sound for the purpose of imaging are analysed.

On the one hand one may attempt to create a bubble via type I nucleation. The pressures required to do so in water are beyond the capabilities of diagnostic ultrasound and so one may instead focus on creating an emulsion with a second medium that is easier to nucleate. The perfluorocarbons, due to their low boiling points, low solubility and low toxicity make excellent candidates. This chapter has suggested by means of the capillary approximation that very few perfluoro-molecules are needed to create a bubble, and that the nucleating pressure is much reduced - down to 7-8 MPa negative pressure for perfluoropentane These pressures are still on the cusp of what is used in medical ultrasound and are still beyond what can be achieved with a diagnostic transducer. However, given the questions regarding the approximation's accuracy that are raised by the calculated number of nucleating molecules - in the tens and low hundreds - the perfluorocarbons still most definitely represent a contrast medium that is worthy of experimental study.

On the other hand one may abandon type I and type II nucleation altogether

and focus on extracting gas that is stabilised in impure water. The main difficulties in this approach is to control the impurities in the water so that small bubbles are not overwhelmed by larger bubbles, and to image the generated bubble within its millisecond lifetime. Generating bubbles at diagnostic pressures is not a challenge in this approach. Indeed, great pains are usually gone through in ultrasound experiments to prevent such bubble generation.

A certain degree of control can be exerted on the size of bubble generated in by type III nucleation. From 2.24 the critical radius of an air bubble is found to be

$$R^* = \frac{2\gamma}{\zeta P_\infty}. \tag{2.26}$$

The Laplace relation, 2.4, cannot be used as it focuses solely on vapour bubbles. The saturation, ζ, can be plotted as a function of pressure by using Henry's law, which finds that density a gas in water is proportional to the applied pressure,

$$P = Hn, \tag{2.27}$$

where H is Henry's constant. One finds that

$$R^* = \frac{2\gamma}{n_0 H - P_\infty}. \tag{2.28}$$

Since the critical radius provides a lower bound on the size of the evacuated bubble, equation 2.26 provides an estimated on the size of bubble that is generated in dirty water.

2.6.2 Concerns with the capillary approximation

The assumptions of the capillary approximation are problematic when the nucleating bubble is very small [105] because the distance over which the density changes from liquid to vapour is not insignificant and because the surface tension is typically reduced from its bulk value [54].

Deviations from the capillary approximation are exponentially important in rate calculations, which follows from the Arrhenius equation. For example, an increase in the surface tension of 15% was calculated [54] to change the predicted nucleation rate by 10^{17}. Another example is provided by the calculations of Talanquer and Oxtoby [78;105]. Their density functional calculations, that relaxes the requirement for sharp interfaces between liquid and vapour, predicted that the rates from these calculations were *typically* 20 orders of magnitude different from those of classical nucleation theory.

The version of the classical nucleation theory used here is perhaps the simplest that can be used. There are many modifications that alter in some way the exponential in 2.11, and thereby drastically altering the rate predictions. The problems of the capillary approximation are common to all classical theories, however, and so the simple application here is representative.

Perhaps the most relevant of the modified classical theories is the careful ap-

plication to bubble nucleation carried out by Delale[16]. In addition to the problems associated with the capillary approximation, Delale notes that it is unlikely in ultrasound applications for cavitation to proceed on a reversible path, as is assumed. Furthermore, the viscous dampening at the bubble-oil interface, which is known to be important in bubble dynamics, mean that at thermodynamic equilibrium (when the bubble's radius is at its critical size), the bubble is not in mechanical equilibrium. Delale[16] convincingly argues for a phenomenological term should be added to the Gibbs energy difference to correct for these problems. Unfortunately the terms of this correction are difficult to ascertain far from the critical temperature. It is therefore difficult to apply Delale's theory in this thesis[16].

2.6.3 Testing the validity of the capillary approximation

For small bubbles, the assumption of a sharp interface between the bubble and its medium is open to criticism. Can the width of the interface really be insignificant for a bubble 50 nm wide? In this section we investigate the issue by taking an alternative approach, the density functional programme of Oxtoby and Evans[78].

Density functional theory relaxes the capillary approximation used in classical nucleation theory. The density of the nucleated bubble is not assumed to be uniform, and the interface is not assumed to be macroscopic and plainer[77;78]. The density functional approach therefore does much better at modelling the interface than classical nucleation theory. Rather than it being a sharp boundary, there is a finite interval over which the density varies from that of the fluid to that of the vapour. In addition, and as will be shown, the energy barrier to the phase change vanishes at the spinodal. This is as it should be, but marks a second major improvement on the classical theory[106].

Density functional theory starts by modelling the inter-molecular potentials. Good models for the fluid potential exist and among the most widely used are the Lennard-Jones potential and the Kihira potential. The former describes small spherically symmetric molecules very accurately. The latter is a extension on the Lennard-Jones model to describe larger, less symmetric molecules.

In principle, macroscopic predictions can then be drawn by inserting the intermolecular potentials into the usual thermodynamic potentials of statistical mechanics. While the full multi-particle potentials are in general insolvable and approximations must be made, the density functional approach is one derived from a firm theoretical base[24]. Unfortunately, when applied to nucleation, the first principles approach has only ever had qualitative success[76;107], with the predictions being very sensitive to the modelled molecular scale parameters.

The semi-empirical approach of Nyquist[76] and Talanquer[107] attempts to temper this sensitivity by fitting the molecular-scale parameters to the experimental data used for the classical theory. By construction, therefore, the bulk thermodynamic predications of the model are correct. Thermodynamic arguments can then be used to obtain other quantities of interest, such as the nucleation rate. We shall use this approach to test the width of interface between the bubble and its medium.

The density functional approach models fluctuations about the bulk properties of the fluid. It is therefore a mean-field approach that fails, like all mean field theories, near to the critical temperature. One must be cautious, therefore, only to apply it to nucleation events that occur well away from the critical point. In this thesis attention is restricted to nucleation events that are induced by a reduction in pressure rather than by boiling. The critical temperatures for a number of perfluorocarbons are listed in Table 2.1. It is interesting to note that for the perfluorocarbons the critical temperatures are considerably higher than their boiling points. At 37 °C, for example, perfluoropentane is in a metastable state but is still far from being 'on the cusp' of vapourisation. Type 1 nucleation events are still likely to occur via a reduction in pressure rather than an increase in temperature. On the other hand, perfluoroethane is above its critical point at room temperature and we consider it to be a little to close to its critical point to be considered in this thesis.

2.6.3.1 Outline of approach

The approach we will be taking can be summarised as follows:

1. write down an accurate model for the intermolecular potential (section 2.6.3.2),
2. approximate the model so that it can be solved (section 2.6.3.3),
3. fit the model's parameters so that it reproduces macroscopic thermodynamics (section 2.6.3.4),
4. predict the shape of the interface between the bubble and its medium and compare it with the capillary approximation (section 2.6.4).

2.6.3.2 The density functional approach

The density functional approach is a statistical theory that attempts to model the grand potential, Ω, at a molecular level. The exact solution is intractable due to the mutual interactions between every molecule in the system.

To overcome this problem the true probability density function, $p_0(\mathcal{H}; \mathbf{r}_1, \mathbf{p}_1)$, that describes the positions of the particles and their momenta, is approximated to a simpler distribution $p(H; \mathbf{r}_1, \mathbf{p}_1)$ that may be solved. Here, $\mathcal{H}$, is the true Hamiltonian of the system and H is the approximate Hamiltonian with simpler interaction terms. We have also employed the convenient shorthand

$$\mathbf{r}_n \equiv r_n, r_{n+1}, \ldots, r_N, \quad \text{and} \quad \mathbf{p}_n \equiv p_n, p_{n+1}, \ldots, p_N. \tag{2.29}$$

to describe the positions and momenta of $N - n$ particles.

The *relative entropy* or *Kullback-Leibler divergance* gives the amount of information lost when using the approximate distribution p rather than the correct distribution p_0, and is defined

$$D_{\mathrm{KL}}\left(p||p_0\right) = \mathrm{Tr} p \log \frac{p}{p_0}, \tag{2.30}$$

where Tr is the classical trace operator. The relative entropy has the property that $D_{\mathrm{KL}}(p||p_0) \geq 0$, which follows from Gibbs inequality [69]. Only if $p = p_0$ does $D_{\mathrm{KL}}(p||p_0) = 0$. Therefore, once the structure of the approximate distribution p has been chosen, it can be varied to match to content of p_0 as closely as possible by minimising $D_{\mathrm{KL}}(p||p_0)$.

Employing this variational procedure to approximate the thermodynamic potentials is ubiquitous in statistical physics [120]. The point of departure for the density functional method is the realisation that

1. the *density is a functional of the external potential.* This follows because the approximation to the density is related to the single particle probability density function

$$\rho(\mathbf{r}) \propto \iint d\mathbf{p}_1 d\mathbf{r}_2 p(H, \mathbf{r}, \mathbf{p}) \propto \int e^{-\beta \sum_i^N V_{\mathrm{ext}}(\mathbf{r}_i)} d\mathbf{r}_2 \tag{2.31}$$

   where $V_{\mathrm{ext}}(\mathbf{r}_i)$ is the external potential at the position $\mathbf{r}$ of the i^{th} molecule. Here were have extended the shorthand employed in 2.32 so that

$$d\mathbf{r}_n \equiv dr_n dr_{n+1} \dots dr_N, \qquad \text{and} \quad d\mathbf{p}_n \equiv dp_n dp_{n+1} \dots dp_N. \tag{2.32}$$

2. *the external potential is uniquely determined by the density.* This converse result is known as the Hohenberg-Kohn theorem. It follows because the external potential is determined by the probability density, p, which is in turn determined uniquely by the density.

It is thereby permissible to work with the mass density rather than the probability density when considering the thermodynamics of the bubble. Since the density is the term of interest, the density functional approach is much more direct. We may therefore define a approximate grand potential, Ω_V, as a functional of the (approximate) density [24],

$$\Omega_V[\rho] \equiv \beta^{-1} D_{\mathrm{KL}}(p[\rho]||p_0) + \Omega. \tag{2.33}$$

The approximate grand potential approaches the true value when it is minimised with respect to ρ. Furthermore, since Ω is the grand potential at thermodynamic equilibrium, Ω_V is minimal when ρ describes the critical density distribution. The condition of equation 2.2 can therefore be expressed by the functional derivative [77]

$$\frac{\delta \Omega_V}{\delta \rho} = 0, \quad \text{at } \rho = \rho^*. \tag{2.34}$$

The grand potential is related to the Helmholtz free energy by a Legendre transformation

$$\Omega_V = F - \mu \int d\mathbf{r} \rho(\mathbf{r}), \tag{2.35}$$

where μ is the chemical potential. The free energy, F, is the sum of internal energy Φ and an entropic contribution. The inter-particle interactions are

contained within the internal energy.

2.6.3.3 Approximate the model

To simplify F it is noted that the interactions of most fluids are dominated by volume exclusion effects (van der Waal type interactions). Longer range interactions are, in general, only of secondary importance [77]. If only pair-wise attractions are considered, then the internal energy can then be split into the free energy of a *hard sphere* reference fluid, F_{hs} and a small perturbation, ϕ_{attr}, that incorporates the long range attractions. Then

$$F[\rho] = F_{\text{hs}}[\rho] + \tfrac{1}{2}\iint d\mathbf{r}_i d\mathbf{r}_j \phi_{\text{attr}}(\mathbf{r}_i, \mathbf{r}_j)\rho(\mathbf{r}_i, \mathbf{r}_j), \tag{2.36}$$

where $\phi_{\text{attr}}(\mathbf{r}_i, \mathbf{r}_j)$ is the residual two particle potential between a particle at $\mathbf{r}_i$ and $\mathbf{r}_j$, not incorporated into F_{hs}. $\rho(\mathbf{r}_i, \mathbf{r}_j)$ is the two particle density function. (See Evans [24] for a formal treatment of the above steps).

Next we model the attractive perturbation. To do so, we begin with a model for the full two particle interaction and then split it into attractive and repulsive parts, according the WCA procedure. For small symmetric molecules the Lennard-Jones 6-12 potential has good accuracy. It is given by

$$\phi_{\text{LJ}}(r) = 4\epsilon\left(\frac{\sigma^{12}}{r^{12}} - \frac{\sigma^6}{r^6}\right) \tag{2.37}$$

where $r = |\mathbf{r} = \mathbf{r}'|$, η is the characteristic bond energy and σ the characteristic length. The Kihira-potential does a better job for larger models such as perfluoropentane but greatly complicates the approach. The Lennard-Jones potential is used in this thesis.

The potentials are then separated into attractive and repulsive parts, ϕ_{attr} and ϕ_{rep}, respectively,

$$\phi_{\text{rep}}^{\text{WCA}}(r) = \begin{cases} \phi(r) + \epsilon & \text{if } r < r_{\min} \\ 0 & \text{otherwise} \end{cases} \tag{2.38}$$

and

$$\phi_{\text{attr}}^{\text{WCA}}(r) = \begin{cases} -\epsilon & \text{if } r < r_{\min} \\ \phi(r) & \text{otherwise} \end{cases} \tag{2.39}$$

where $r_{\min}$ is the radius at which the potential is minimal.

It is useful at this stage to define the integrated strength of the attractive potential,

$$\alpha = -\iint d\mathbf{r}_i d\mathbf{r}_j \phi_{\text{attr}}(\mathbf{r}_i, \mathbf{r}_j). \tag{2.40}$$

Finally to reestablish contact with the hard sphere approximation the repulsive part of the decomposition is replaced by an infinite repulsion at a distance d,

That is

$$\phi_{\text{hs}}(r) = \begin{cases} \infty & \text{if } r < d \\ 0 & \text{otherwise} \end{cases} . \tag{2.41}$$

Equation 2.36 is still exact for two particle potential theories. In order to solve it we first assume that the hard sphere potential is a function only of the local density,

$$F_{\text{hs}}[\rho] \approx \int d\mathbf{r} f_{\text{hs}}(\rho(\mathbf{r})). \tag{2.42}$$

$f_{\text{hs}}(\rho(\mathbf{r}))$ is the potential (per unit volume) of a uniform hard-sphere fluid [24]. It is obtained from the accurate Carnahan-Stirling equation of state,

$$f_h(\rho(\mathbf{r})) = f_{\text{ideal}} + \rho k_B T \frac{4\eta - 3\eta^2}{(1-\eta)^2} \tag{2.43}$$

where $\eta = \frac{\pi \rho d^3}{6}$ is the packing function and $f_{\text{ideal}} = \rho k_B T \left(\ln\left(\rho\lambda^3\right) - 1\right)$ is the free energy (per volume) of an ideal gas. λ is the de Broglie wavelength. The approximation 2.42 is known as the *local-density approximation.*

The perturbation may be approximated by assuming that the two particle densities are uncorrelated,

$$\rho(\mathbf{r}_i, \mathbf{r}_j) \approx \rho(\mathbf{r}_i)\rho(\mathbf{r}_j). \tag{2.44}$$

This is known as the *random phase approximation.* If the medium is sufficiently large then this approximation should hold [24]. The random phase approximation may well need to be refined for very small oil droplet in water, where the oil-water interface cannot be ignored.

Equation 2.35 can therefore be written as an explicit function of ρ,

$$\Omega_V = \int d\mathbf{r} f_{\text{hs}}(\rho(\mathbf{r})) + \iint d\mathbf{r}_i d\mathbf{r}_j \phi_{\text{attr}}(\mathbf{r}_i, \mathbf{r}_j)\rho(\mathbf{r}_i)\rho(\mathbf{r}_j) - \mu \int d\mathbf{r}\rho(\mathbf{r}), \tag{2.45}$$

where equations 2.36, 2.42 and 2.44 have been used. Minimising 2.45 with respect to $\rho(\mathbf{r})$ gives

$$\frac{\delta f_{\text{hs}}(\rho(\mathbf{r}))}{\delta\rho(\mathbf{r})} \equiv \mu_{\text{hs}}[\rho(\mathbf{r})] = \mu - \int d\mathbf{r}' \phi_{\text{attr}}(\mathbf{r}, \mathbf{r}')\rho(\mathbf{r}'). \tag{2.46}$$

$\mu_{\text{hs}}[\rho(\mathbf{r})]$ is the chemical potential of the hard sphere fluid[2].

All the terms on in 2.46 can be obtained for a given function density profile. μ_{hs} on the left and the second term on the right hand side have explicit rep-

[2]The chemical potential of a hard sphere fluid is given by

$$\mu_{\text{hs}} = \frac{df_h}{d\rho} = k_B T \frac{8\eta - 9\eta^2 + 3\eta^3}{(1-\eta)^3} + k_B \ln\left(\rho\lambda^3\right) \tag{2.47}$$

resentations, while the chemical potential μ 'mean field' obtained by analysing the bulk properties of the fluid. Equation 2.46 can therefore be solved by iteration. An initial guess as the density profile is given to the right hand side. The chemical potential $\mu_{\rm hs}$ is then inverted (numerically) to give an improved estimate of ρ.

The density obtained by solving 2.46 is the density that minimises Ω_V, and it therefore gives the best approximation the true equilibrium grand potential. The bubble is only in thermodynamic equilibrium when it is at its critical radius. Therefore the density ρ obtained from 2.46 is the density profile of the critical bubble.

2.6.3.4 Fit the model parameters

To use equation 2.46 we need to define the free parameters in our model. There are four parameters in total, of which three are independent,

1. ϵ - the energy scale in the Lennard-Jones 6-12 potential (equation 2.37),
2. σ - the length scale in the Lennard-Jones 6-12 potential (equation 2.37),
3. α - the attractive stength of the Lennard-Jones 6-12 potential (equation 2.40),
4. d - The length scale in the hard-sphere model (equation 2.43).

Two of the parameters can be set by considering the bulk fluid. If the density is uniform then equation 2.45 becomes

$$\Omega_V/V = f_{\rm hs}(\rho) - \tfrac{1}{2}\alpha\rho^2 - \mu\rho = p_{\rm hs} + \mu_{\rm hs}\rho - \tfrac{1}{2}\alpha\rho^2 - \mu\rho. \tag{2.48}$$

where V is the volume of the system[3].

Equation 2.48 can be minimised with the help of the Maxwell relation

$$\frac{\partial\, p_{\rm hs}}{\partial\, \rho} = \rho\frac{\partial\, \mu_{\rm hs}}{\partial\, \rho} \tag{2.50}$$

to obtain

$$\mu = \mu_{\rm hs} - \alpha\rho. \tag{2.51}$$

Substituting 2.51 into 2.48 gives

$$\Omega_V/V = -p_{\rm hs}(\rho) + \tfrac{1}{2}\alpha\rho^2 = -p. \tag{2.52}$$

Equation 2.52 depends only on d and α.

[3]The hard sphere pressure is given by

$$p_{\rm hs} = k_B T\rho\frac{1+\eta+\eta^2-\eta^3}{1-\eta^3}. \tag{2.49}$$

Below the critical temperature there will be two phases in bulk coexistence. The number densities of these two phases are ρ_v and ρ_L, where the "v" denotes the vapour and the "L" denotes the liquid. At equilibrium the chemical potential and the pressures for both phases are equal

$$\mu_v = \mu_{\text{hs}}(\rho_v) - \alpha\rho_v = \mu_{\text{hs}}(\rho_L) - \alpha\rho_L = \mu_L, \tag{2.53a}$$

$$p_v = p_{\text{hs}}(\rho_v) - \tfrac{1}{2}\alpha\rho_v^2 = p_{\text{hs}}(\rho_L) - \tfrac{1}{2}\alpha\rho_L^2 = p_L. \tag{2.53b}$$

The solutions of equations 2.53 define the coexistance curve for the fluid, and they may be used to obtain the two parameters d and α.

The final parameter, σ (or equivalently ϵ) is obtained from the measured surface tension of the fluid. The value of Ω is obtained by iterating 2.46. The surface tension is then calculated by noting that

$$\Omega_V = \Omega_{V_l} + \Omega_{V_g} + \gamma A, \tag{2.54}$$

where Ω_{V_l} and Ω_{V_g} are the potentials of the bulk liquid and gas evaluated at the Gibbs surface, γ is the surface tension and A is the area of the surface. The value of σ is chosen so that the calculated value of γ matches its experimental value.

The code to solve these equations was written by the author of this thesis and is freely available on github[97].

2.6.4 Results of the density functional approach

2.6.4.1 The coexistence curve

The coexistence curve for water and perfluoropentane are plotted in Figure 2.5. The experimental values that are used to make the fit are shown with points, and the computed curve is shown with a solid line. The fit for the vapour was used to obtain d and ϵ for the model and so is by definition exact. The quality of the model can be assessed by comparing the experimental values for the liquid with the fit. It is seen to be highly accurate away from the critical point, at which point theory and experiment start to diverge.

The calculated spinodal is also plotted in Figure 2.5. The spinodal is defines the point of equilibrium where the energy barrier to the transition vanishes (see Favvas[26] for an introduction). There region of the spinodal is bound by the curves

$$\mu_v = \mu_{\text{hs}}(\rho_v) - \alpha\rho_v = \mu_{\text{hs}}(\rho_L) - \alpha\rho_L = \mu_L, \tag{2.55a}$$

$$\frac{\partial\,\mu_v}{\partial\,\rho} = 0 \tag{2.55b}$$

$$\text{or} \quad \frac{\partial\,\mu_L}{\partial\,\rho} = 0 \tag{2.55c}$$

Equation 2.55a demands thermodynamic equilibrium. Equation 2.55b ad 2.55c demand that the equilibrium point is a saddle point (where the energy barrier

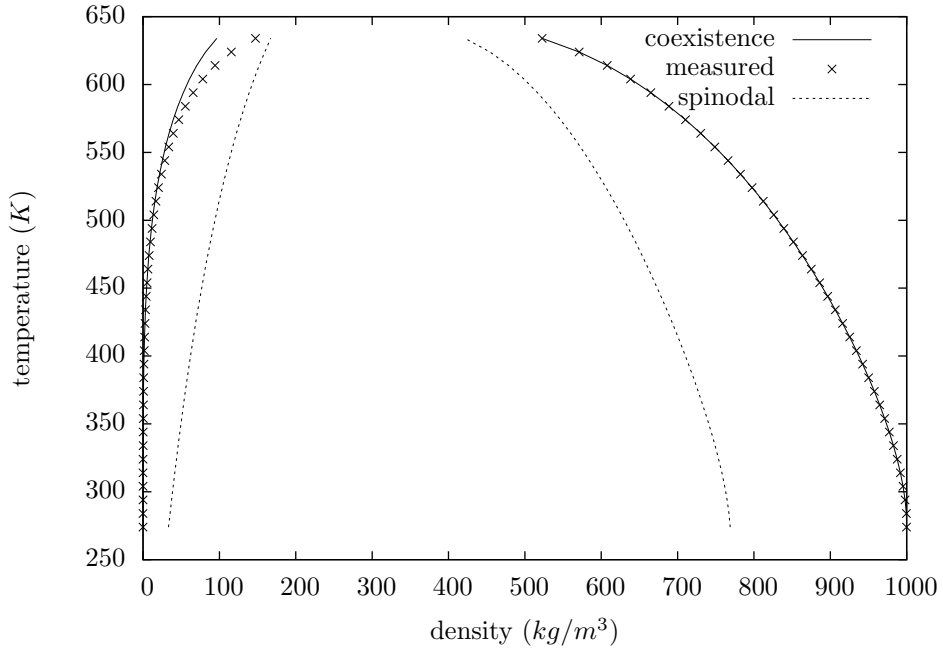

(a) Coexistence for water

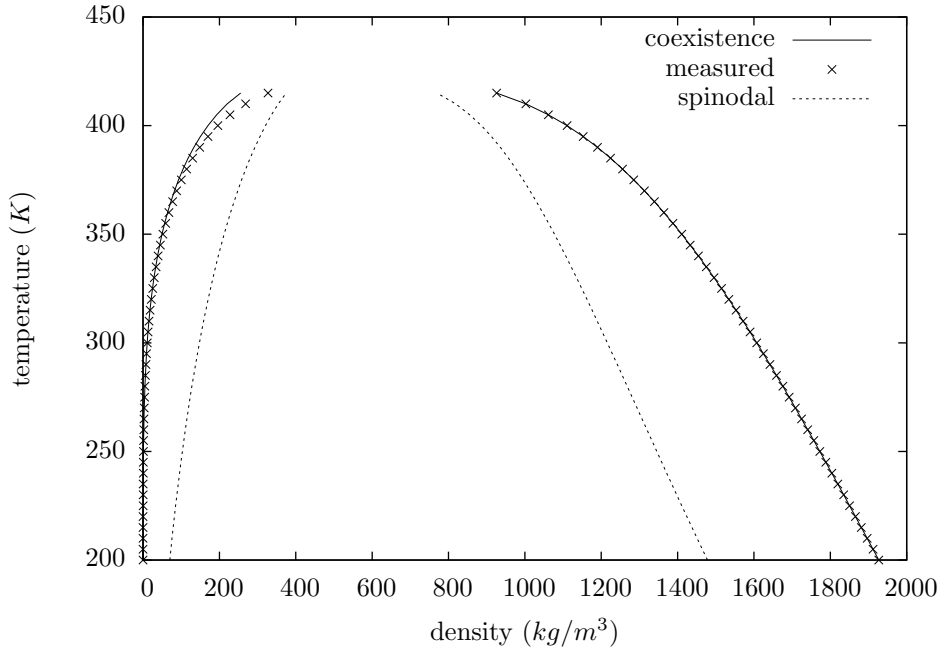

(b) Coexistence for perfluoropentane

Figure 2.5: Coexistence and spinodal curve for water and perfluoropentane. The plot was used to obtain the temperature dependence of the parameters d and ϵ in the hard-sphere model with Lennard-Jones interactions.

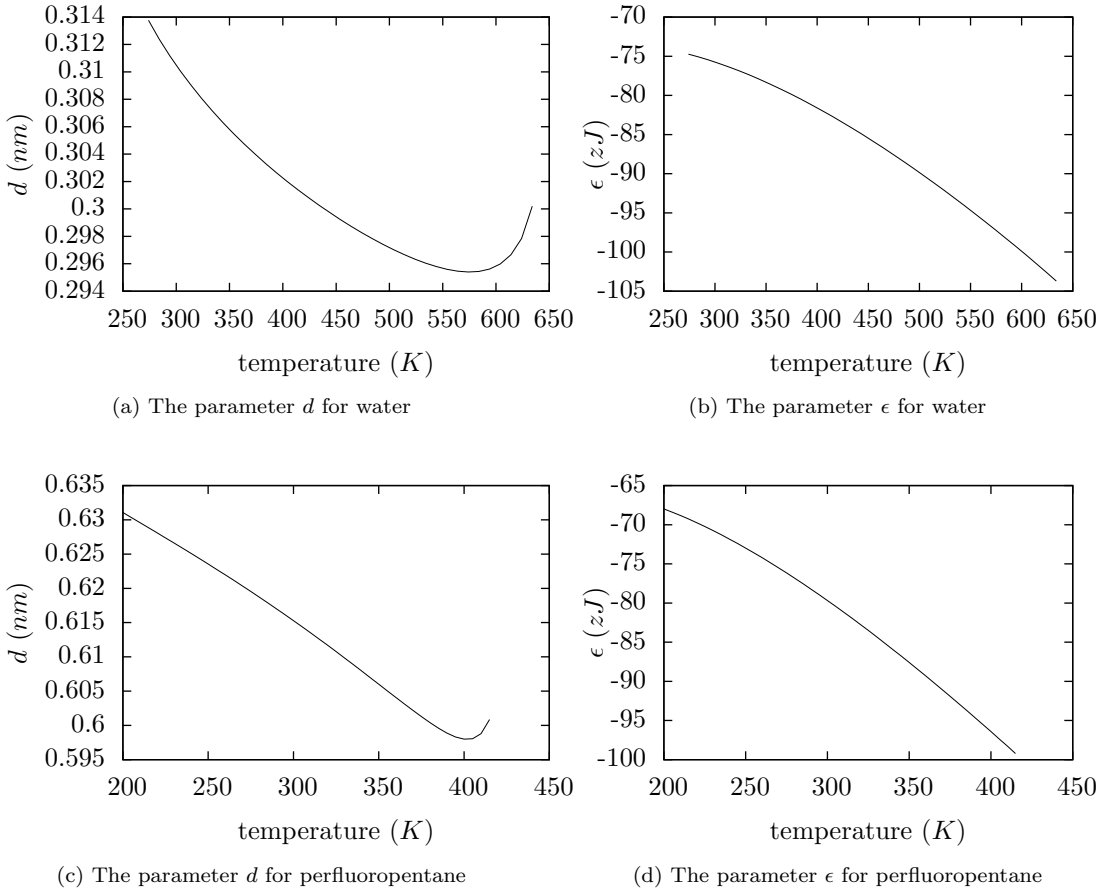

(a) The parameter d for water

(b) The parameter ϵ for water

(c) The parameter d for perfluoropentane

(d) The parameter ϵ for perfluoropentane

Figure 2.6: A plot of the temperature dependence of the parameters d and ϵ in the hard-sphere model with Lennard-Jones interactions.

vanishes). While the decomposition of phases past the spinodal is not nucleation - the phases separate throughout the medium rather than forming a bubble - the spinodal nevertheless marks a fundamental and guaranteed change in the medium that is surely detectable.

The fitted values of d and *epsilon* are plotted in Figure 2.6. The stability of the parameters below the critical point is encouraging for it indicates that the predictive power of the parameters is strong. Near the critical point the curve in starting to be very sensitive changes in temperature. The model is not applicable near the critical point and its parameters are being pulled inappropriately by the changing physics.

The parameters at 20° are plotted in Table 2.4. One notable observation is that the distance scale in the Lennard-Jones model is very small for water. This indicates a very low interaction length. The reason for this is the highly polar nature of water. Density functional approaches have previously been found to struggle in the presence of highly polar fluids such as water[76;107], with the

Table 2.4: Density functional parameters for perfluoropentane and water at 20°

	perfluoropentane	water
ϵ	-80 zJ	-76 zJ
d	0.61 nm	0.31 nm
σ	0.41 nm	0.016 nm

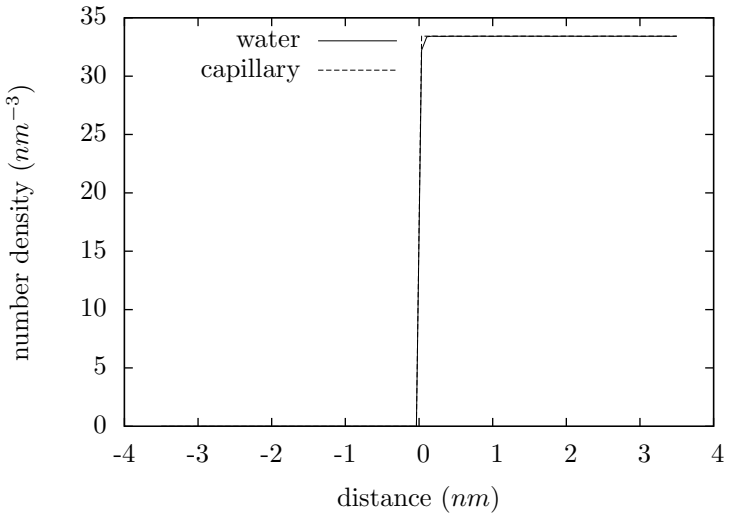

(a) Density profile at the interface of water

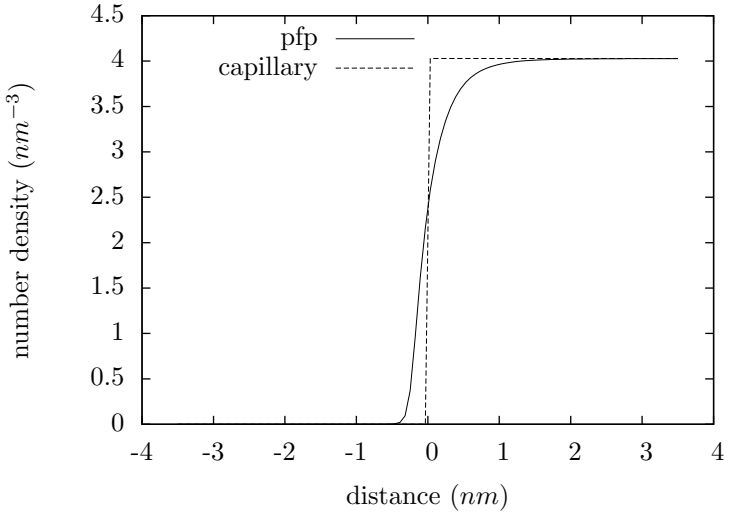

(b) Density profile at the interface of perfluoropentane

Figure 2.7: The plainer density profiles of water and perfluoropentane at 293 K.

same consequence for the value of d.

In Figure 2.7 the density profiles for water and perfluoropentane are plotted. The small value of d for water means that the density profile varies over very rapidly and is essentially indistinguishable from the apillary approximation. The are box expected to perform equally poorly.

From Figure 2.7b it is seen that the density profile for perfluoropentane varies over a more significant length scale. The 1 nm of Figure 2.7b represents approximately 10% of the critical radius of a perfluoropentane vapour droplet under 1 MPa tension. The use of the capillary approximation for perfluoropentane is therefore highly questionable.

2.6.5 Further work

The density profile of perfluoropentane plotted in Figure 2.7b indicates that the density functional approach may have much to offer theoretical studies of perfluoropentane.

In particular, the density functional approach can be extended to binary fluids[107] to estimate the nucleation rates for various gases dissolved within the perfluorpentane droplet. The perfluorocarbons are remarkable for their solubility of carbon dioxide. It could be that type 1 nucleation can be facilitated by the perfluorocarbons not by their low boiling points, but rather due to the nucleation of their dissolved gases.

Bibliography

[1] *Convertible Liquid Droplets for Ultrasound Contrast*, Rotterdam, The Netherlands, January 2010. 15th EUROPEAN SYMPOSIUM ON ULTRASOUND CONTRAST IMAGING.

[2] R.G.W. Anderson. Caveolae - where incoming and outgoing messengers meet. *Proceedings of the National Academy of Sciences of the United States of America*, 90(23):10909–10913, Dec 1993.

[3] B. Anglesen and R. Hansen. Surf imaging a new method for ultrasound contrast agent imaging. pages 531–541. IEEE Ultrasonics Symposium Proceedings, 2007.

[4] R.E. Apfel. Acoustic cavitation inception. *Ultrasonics*, 22(4):167 – 173, 1984. ISSN 0041-624X. doi: DOI: 10.1016/0041-624X(84)90032-5.

[5] A. A. Atchley and A. Prosperetti. The crevice model of bubble nucleation. *Acoustical Society of America Journal*, 86:1065–1084, September 1989. doi: 10.1121/1.398098.

[6] B. Ballou, B.C. Lagerholm, L.A. Ernst, M.P. Bruchez, and A.S. Waggoner. Noninvasive imaging of quantum dots in mice. *Bioconjugate Chemisty*, 15(1):79–86, 2004.

[7] Carlos Barceló, Stefano Liberati, and Matt Visser. Analogue gravity. *Living Reviews in Relativity*, 8:12, 2005. arXiv:gr-qc/0505065v2.

[8] Charles Baudelaire. The painter of modern life. In Jonathan Mayne, editor, *The Painter of Modern Life and Other Essays*. London: Phaidon Press, 1995.

[9] Vilhelm Bjerknes. *Fields of Force: Supplimentary lectures, applications to meteorology*. Cornell University Library, 1991, 1905.

[10] S.H. Bloch, R.E. Short, K.W. Ferrara, and E.R. Wisner. The effect of size on the acoustic response of polymer-shelled contrast agents. *Ultrasound in Medicine and Biology*, 31(3):439–444, Mar 2005.

[11] Bram M. Borkent, Stephan M. Dammer, Holger Schönherr, G. Julius Vancso, and Detlef Lohse. Superstability of surface nanobubbles. *Phys. Rev. Lett.*, 98(20):204502, May 2007. doi: 10.1103/PhysRevLett.98.204502.

[12] Bram M. Borkent, Stephan Gekle, Andrea Prosperetti, and Detlef Lohse. Nucleation threshold and deactivation mechanisms of nanoscopic cavitation nuclei. *Physics of Fluids*, 21(10):102003, 2009. doi: 10.1063/1.3249602.

[13] CGPM Comptes Rendus of the Conférence Générale des Poids et Mesures. The 17th conférence générale des poids et mesures, 1984, 20, 25.

[14] Oliver Couture, Peter D. Bevan, Emmanuel Cherin, Kevin Cheung, Peter N. Burns, and F. Stuart Foster. Investigating perfluorohexane particles with high-frequency ultrasound. *Ultrasound in Medicine and Biology*, 32(1):71–82, 2006.

[15] R. T. Cox. Probability, frequency and reasonable expectation. *American Journal of Physics*, 14(1):1–13, January-February 1946.

[16] Can F. Delale, Jan Hruby, and Frantisek Marsik. Homogeneous bubble nucleation in liquids: The classical theory revisited. *The Journal of Chemical Physics*, 118(2):792–806, 2003. doi: 10.1063/1.1525797.

[17] Alexander A. Doinikov, Paul S. Sheeran, Ayache Bouakaz, and Paul A. Dayton. Vaporization dynamics of volatile perfluorocarbon droplets: A theoretical model and in vitro validation. *Medical Physics*, 41 (10):102901, 2014. doi: http://dx.doi.org/10.1118/1.4894804. URL `http://scitation.aip.org/content/aapm/journal/medphys/41/10/10.1118/1.4894`

[18] Carl E. Dolby and Stephen F. Gull. On radar time and the twin 'paradox'. *American Journal of Physics*, 69(12):1257–1261, October 2001.

[19] Chris Doran and Anthony Lasenby. *Geometric Algebra for Physicists*. Cambridge University Press, 2003.

[20] A. Einstein. Zur elektrodynamik bewegter körper. *Annalen der Physik*, 17:891–921, 1905. English translation available in *The Priciple of Relativity*, Dover, 1952.

[21] P. S. Epstein and M. S. Plesset. On the stability of gas bubbles in liquid-gas solutions. *Journal of Chemical Physics*, 18(11):1505–1509, 1950.

[22] Lina Du et al. Ultrasound-triggered drug release and enhanced anticancer effect of doxorubicin-loaded poly(d,l-lactide-co-glycolide)-methoxy-poly(ethylene glycol) nanodroplets. *Ultrasound in Medicine and Biology*, 37(8):1252–1258, 2011.

[23] Natalya Rapoport et al. Cavitation properties of block copolymer stabilized phase-shift nanoemulsions used as drug carriers. *Ultrasound in Medicine and Biology*, 36:419–429, 2007.

[24] R Evans. Density functionals in nonuniform fluids. In D Henderson, editor, *Fundamentals of Inhomogeneous Fluids*, pages 85–175. Marcel Dekker, Inc, 1992.

[25] Mario L. Fabiilli, Kevin J. Haworth, Ian E. Sebastian, Oliver D. Kripfgans, Paul L. Carson, and J. Brian Fowlkes. Delivery of chlorambucil using an acoustically-triggered perfluoropentane emulsion. *Ultrasound in Medicine & Biology*, 36(8):1364 – 1375, 2010. ISSN 0301-5629. doi: DOI: 10.1016/j.ultrasmedbio.2010.04.019.

[26] P. Favvas and A. Ch. Mitropoulos. What is spinodal decomposition? *Journal of Engineering Science and Technology Review*, 1:25–27, 2008.

[27] Katherine Ferrara, Rachel Pollard, and Mark Borden. Ultrasound microbubble contrast agents: Fundamentals and application to gene and drug delivery. *Annual Review of Biomedical Engineering*, 9(1):415–447, 2007. doi: 10.1146/annurev.bioeng.8.061505.095852.

[28] L. M. Fisher. Company news; f.d.a. approves compound for heart scans. New York Times, 09 August 1994.

[29] M. Foucault. What is enlightenment. In P. Rabinow, editor, *The Foucault Reader*. Penguin Books, 1984, 1978.

[30] Y. Fukumori and H. Ichikawa. Nanoparticles for cancer therapy and diagnosis. *Advanced Powder Technology*, 17(1):1–28, 2006.

[31] M. S. Garrido. Note sur la mécanique relativiste des fluides incompressibles. *Il Nuobo Cimento*, 68B(2):252–260, Apr 1982.

[32] T. Giesecke and K. Hynynen. Ultrasound-mediated cavitation thresholds of liquid perfluorocarbon droplets in vitro. *Ultrasound in Medicine and Biology*, 29(9):1359–1365, Sep 2003.

[33] Peter Goldreich, Sanjoy Mahajan, and Sterl Phinney. *Order-of-Magnitude Physics: Understanding the World with Dimensional Analysis, Educated Guesswork, and White Lies*. unpublished, 1999.

[34] Gennady Yu. Gor, Anatoly E. Kuchma, and Fedor M. Kuni. Gas bubble growth dynamics in a supersaturated solution: Henry's and sievert's solubility laws. *JINR Dubna*, pages 213–233, 2011. arXiv:1205.5471 [physics.chem-ph].

[35] H. Hashizume, P. Baluk, and S. Morikawa et al. Openings between defective endothelial cells explain tumor vessel leakiness. *American Journal of Pathology*, 156(4):1363–1380, Apr 2000.

[36] Edvard A. Hemmingsen. Cavitation in gas - supersaturated solutions. *Journal of Applied Physics*, 46(1):213–218, 1975. doi: 10.1063/1.321323.

[37] Eric Herbert, Sébastien Balibar, and Frédéric Caupin. Cavitation pressure in water. *Phys. Rev. E*, 74(4):041603, Oct 2006. doi: 10.1103/PhysRevE.74.041603.

[38] D. Hestenes. Spacetime physics with geometric algebra. *American Journal of Physics*, 71(7):691–714, July 2003.

[39] David Hestenes and Garret Sobczyk. *Clifford Algebra to Geometric Calculus: A Unified Language for Mathematics and Physics*. D. Reidel Publishing Company, Kluwer Academic Publishers Group, 1984.

[40] S.K. Hobbs, Wayne L. Monsky, Fan Yuan, W. Gregory Robertspar, Linda Griffithdagger, Vladimir P. Torchilin, and Rakesh K. Jain. Regulation of transport pathways in tumor vessels: Role of tumor type and microenvironment. *Proceedings of the National Acadamy of Sciences of the United States of America*, 95(8):4607–4612, Apr 1998.

[41] L Hoff. *Acoustic Characterisation of Contrast Agents for Medical Ultrasound Imaging*. Kluser Academic Publishers, 2001.

[42] M. S. Howe. *Acoustics of Fluid-Structure Interactions*. Cambridge Monographs on Mechanics. Cambridge University Press, 1998.

[43] M. S. Howe. *Theory of Vortex Sound*. Cambridge Texts in Applied Mathematics. Cambridge University Press, 2003.

[44] J.A. Copland JA, M. Eghtedari, V.L. Popov VL, N. Kotov, N. Mamedova, M. Motamedi, and A.A. Oraevsky AA. Bioconjugated gold nanoparticles as a molecular based contrast agent: Implications for imaging of deep tumors using optoacoustic tomography. *Molecular Imaging and Biology*, 6(5):341–349, Sep-Oct 2004.

[45] Thomas J. Jarvis, Marc D. Donohue, and Joseph L. Katz. Bubble nucleation mechanisms of liquid droplets superheated in other liquids. *Journal of Colloid and Interface Science*, 50(2):359–368, 1975. ISSN 0021-9797. doi: DOI: 10.1016/0021-9797(75)90240-4.

[46] E. T. Jaynes. Where do we stand on maximum entropy? In R. D. Levine and M. Tribus, editors, *The Maximum Entropy Formalism*, page 15. M.I.T. Press, Cambridge, MA, 1979.

[47] Edwin T. Jaynes. The well-posed problem. *Foundations of Physics*, 3: 477–493, 1973.

[48] Bruce D. Johnson and Robert C. Cook. Generation of Stabilized Microbubbles in Seawater. *Science*, 213(4504):209–211, 1981. doi: 10.1126/science.213.4504.209.

[49] S. F. Jones, G. M. Evans, and K. P. Galvin. Bubble nucleation from gas cavities – a review. *Advances in Colloid and Interface Science*, 80(1):27 – 50, 1999. ISSN 0001-8686. doi: DOI: 10.1016/S0001-8686(98)00074-8.

[50] JL Katz. Homogeneous nucleation theory and experiment - a survey. *Pure and applied chemistry*, 64(11):1661–1666, Nov 1992. ISSN 0033-4545. 7TH International conference on surface and colloid science, Compiegne, France, JUL 07-13, 1991.

[51] Joseph L. Katz and Milton Blander. Condensation and boiling: Corrections to homogeneous nucleation theory for nonideal gases. *Journal of Colloid and Interface Science*, 42(3):496–502, 1973. ISSN 0021-9797. doi: DOI: 10.1016/0021-9797(73)90035-0.

[52] Joseph B. Keller and Michael Miksis. Bubble oscillations of large amplitude. *Journal of the Acoustical Society of America*, 68(2):628–633, Aug 1980.

[53] I.A. Khalil, K. Kogure, and H. Akita et al. Uptake pathways and subsequent intracellular trafficking in nonviral gene delivery. *Pharmacological Reviews*, 58(1):32–45, Mar 2006.

[54] C.S. Kiang, D. Stauffer, G.H Walker, O.P. Puri, J.D Wise, and E.M. Patterso. Reexamination of homogeneous nucleation theory. *Journal of the atmospheric sciences*, 28(7):1222–&, 1971. ISSN 0022-4928.

[55] Kevin H. Knuth. Lattice duality: The origin of probability and entropy. *Neurocomputing*, 67:245–274, 2005.

[56] Kevin H. Knuth and John Skilling. Foundations of inference. *Axioms*, 1 (1):38–73, 2012.

[57] O. D. Kripfgans, J. B. Fowlkes, D. L. Miller, O. P. Eldevik, and P. L. Carson. Acoustic droplet vaporization for therapeutic and diagnostic applications. *Ultrasound in Medison and Biology*, 26(1177-1189), 2000.

[58] O.D. Kripfgans, J.B. Fowlkes, M. Woydt abd O.P. Eldevik, and P.L. Carson. In vivo droplet vaporization for occlusion therapy and phase aberration correction. *IEEE Transactions on Ultrasonics Ferroelectrics and Frequency Control*, 49(6):726–738, Jun 2002.

[59] O.D. Kripfgans, M.L. Fabiilli, P.L. Carson, and J.B. Fowlkes. On the acoustic vaporization of micrometer-sized droplets. *Journal of the Acoustical Society of America*, 116(1):272–281, Jul 2004.

[60] L.D. Landau and E.M. Lifshitz. *Fluid Mechanics*. Number 6 in Course of Theoretical Physics. Elsevier Butterworth Heinemann, 2nd edition, 1987.

[61] A.N. Lasenby, C.J.L. Doran, and S.F. Gull. A multivector derivative approach to lagrangian field theory. *Foundations of Physics*, 23(10):1295–1327, 1993.

[62] M. J. Lighthill. On sound generated aerodynamically. i. general theory. *Proc. R. Soc. Lond. A*, 211(1107):564–587, 20 March 1952.

[63] Chung-Yin Lin and William G. Pitt. Acoustic droplet vaporization in biology and medicine. *BioMed Research International*, 2013. doi:10.1155/2013/40436.

[64] P.J. Linstrom and W.G. Mallard, editors. *NIST Chemistry WebBook, NIST Standard Reference Database*. Number 69. National Institute of Standards and Technology, Gaithersburg MD, 20899, 2010.

[65] Stig Ljunggren and Jan Christer Eriksson. The lifetime of a colloid-sized gas bubble in water and the cause of the hydrophobic attraction. *Colloids and Surfaces A: Physicochemical and Engineering Aspects*, 129-130:151 – 155, 1997. ISSN 0927-7757. doi: DOI: 10.1016/S0927-7757(97)00033-2. Prof. B. W. Ninham.

[66] S. D. Lubetkin. The fundamentals of bubble evolution. *Chem. Soc. Rev.*, 24:243–250, 1995. doi: 10.1039/CS9952400243.

[67] Jacques Lusseyran. *Against the pollution of the I.* Morning Light Press, 2006. Essay entitled: The Blind in Society.

[68] D.J.C. MacKay. *Information Theory, Inference & Learning Algorithms*. Cambridge University Press, 2003.

[69] D.J.C. MacKay. *Information Theory, Inference & Learning Algorithms*. Cambridge University Press, 2003.

[70] Haralabos Marmanis. *Analogy between the Electromagnetic and Hydrodynamic Equations: Appliaton to Turbulence*. PhD thesis, Brown University, 2000.

[71] J. C. Maxwell. On physical lines of force. *The London, Edinburgh and Dublin Philosophical Magazine and Journal of Science*, pages 161–175, March 1861.

[72] G.M. Lanza MD, P.M. Winter, S.D. Caruthers, A.M. Morawskia, A.H. Schmiedera, K.C. Crowder, and S.A. Wickline. From bench to imaging: Magnetic resonance molecular imaging with nanoparticles. *Journal of Nuclear Cardiology*, 11(6):733–743, 2004.

[73] H. K. Moffatt. The degree of knottedness in tangled vortex lines. *Journal of Fluid Mechanics*, 35(1):117–129, 1969.

[74] H. K. Moffatt. Generalised vortex rings with and without swirl. *Fluid Dynamics Research*, 3:22–30, 1988.

[75] J. A. Nelder and R. Mead. A simplex method for function minimization. *Computer Journal*, 7:308–313, 1965.

[76] R.M. Nyquist, V. Talanquer, and D.W. Oxtoby. Density-functional theory of nucleation - a semiempirical approach. *Journal of Chemical Physics*, 103(3):1175–1179, JUL 15 1995. ISSN 0021-9606.

[77] David W. Oxtoby. Nucleation. In D Henderson, editor, *Fundamentals of Inhomogeneous Fluids*, pages 407–442. Marcel Dekker, Inc, 1992.

[78] David W. Oxtoby and R. Evans. Nonclassical nucleation theory for the gas–liquid transition. *The Journal of Chemical Physics*, 89(12):7521–7530, 1988. doi: 10.1063/1.455285.

[79] Hong-Chul Park, Ki-Taek Byun, and Ho-Young Kwak. Explosive boiling of liquid droplets at their superheat limits. *Chemical Engineering Science*, 60(7):1809 – 1821, 2005. ISSN 0009-2509. doi: DOI: 10.1016/j.ces.2004.11.010.

[80] C. L. Pekeris. A relativistic spherical vortex. *Proceedings of the National Academy of Sciences of the United States of America*, 73(3):687–691, March 1976.

[81] C. L. Pekeris. Relativistic axially symmetric flows of a perfect fluid. *Proceedings of the Royal Society of London. Series A, Mathematical and Physical Sciences*, 355(1680):53–60, Jun. 30 1977.

[82] Y.G.A Pierseaux. Einstein's quantum clocks and poincare's classical clocks in special relativity. arXiv:quant-ph/0101146v1, 2001.

[83] Yves Pierseaux. Special relativity: Einsteins spherical waves versus poincaré ellipsoidal waves. *Annales de la Fondation Louis de Broglie*, 30(3-4):353–379, 2005.

[84] Henri Poincaré. La mesure du temps. *Revue de mtaphysique et de morale 6*, 1898. English translation used: The Foundations of Science (The Value of Science) 1913, New York: Science Press, Translator: George Bruce Halsted.

[85] Henri Poincaré. *Science and Hypothesis*. English translation used: The Walter Scott Translation Co. Ltd. 1905, 1902.

[86] Henri Poincaré. Sur la dynamique de l'électron. *Rendiconti del Circolo Matematico di Palemo*, 21:129–175, 1906. English translation for part 1 (used here) available from H.M. Schwartz, American Journal of Physics, November 1971, Volume 39, 1287–1294.

[87] Henri Poincaré. La dynamique de l'électron. *Revue gnrale des sciences pures et appliques*, 19:386–402, 1908.

[88] Henri Poincaré. *The Foundations of Science (Science and Method: Book2)*. Science and Education. New York: Science Press, 1913. Translator: George Bruce Halsted.

[89] Karl Popper. *The Logic of Scientific Discovery*. Routledge Classics, 2002, 1934.

[90] Antonio F. Rañada. Topological electromagnetism. *J. Phys. A: Math. Gen.*, 25:1621, 1992. doi: DOI: 10.1088/0305-4470/25/6/020.

[91] Antonio F. Rañada and José Trueba. Topological electromagnetism with hidden nonlinearity. In Myron W. Evans, editor, *Modern Nonlinear Optics, Part III*, volume 119 of *Advances in Chemical Physics*, pages 197–253. John Wiley & Sons, Inc., 2nd edition, 2002.

[92] Natalya Rapoport, Zhonggao Gao, and Anne Kennedy. Multifunctional nanoparticles for combining ultrasonic tumor imaging and targeted chemotherapy. *J. Natl. Cancer Inst.*, 99:1095–1106, 2007.

[93] K. Sarkar, A. Katiyar, and P. Jain. Growth and dissolution of an encapsulated contrast microbubble: effects of encapsulation permeability. *Ultrasound in Medicine and Biology*, 35(8):1385–1396, Aug 2009.

[94] Kelly C Schad. Characterization of perfluorocarbon droplets for focused ultrasound therapy. Master's thesis, University of Toronto, 2009.

[95] Paul S Sheeran, Terry O Matsunaga, and Paul A Dayton. Phase-transition thresholds and vaporization phenomena for ultrasound phase-change nanoemulsions assessed via high-speed optical microscopy. *Physics in Medicine and Biology*, 58(13):4513, 2013. URL `http://stacks.iop.org/0031-9155/58/i=13/a=4513`.

[96] T.H. Shorrock. hardware. Available on https://github.com/thshorrock, 2012.

[97] T.H. Shorrock. Dft. Available on https://github.com/thshorrock, 2012.

[98] Oleksandr Shpak, Laura Stricker, Michel Versluis, and Detlef Lohse. The role of gas in ultrasonically driven vapor bubble growth. *Physics in Medicine and Biology*, 58(8):2523, 2013. URL `http://stacks.iop.org/0031-9155/58/i=8/a=2523`.

[99] V.A. Shutilov. *Fundalmental Physics of Ultrasound*. Gordaon and Breach Science Publishers, 1988.

[100] John Skilling. Fundamentals of maxent in data analysis. In B. Buck and V. A. Macaulay, editors, *Maximum Entropy in Action: A Collection of Expository Essays*. Oxford University Press, 1991.

[101] L.M Skinner and J.R Sambles. The kelvin equation–a review. *Journal of Aerosol Science*, 3(3):199 – 210, 1972. ISSN 0021-8502. doi: DOI: 10.1016/0021-8502(72)90158-9.

[102] S. Sridhar. Turbulent transport of a tracer: An electromagnetic formulation. *Physical Review E*, 58(1):522–525, July 1998.

[103] HPV Robust Summaries and Test Plan. Cas #86508-32-1 pefluoro compounds, c5-c18, including cas#311-89-7 perfluorotributyl amine. CAS.

[104] V. Talanquer and D. W. Oxtoby. A density-functional approach to nucleation in micellar solutions. *The Journal of Chemical Physics*, 113(16): 7013–7021, 2000. doi: 10.1063/1.1288271.

[105] V. Talanquer and D.W. Oxtoby. Nucleation of Bubbles in Binary Fluids. *Journal of Chemical Physics*, 102(5):2156–2164, Feb 1 1995. ISSN 0021-9606.

[106] V Talanquer and DW Oxtoby. Nucleation in the presence of an amphiphile: A density functional approach. *JOURNAL OF CHEMICAL PHYSICS*, 106(9):3673–3680, MAR 1 1997. ISSN 0021-9606.

[107] V Talanquer, C Cunningham, and DW Oxtoby. Bubble nucleation in binary mixtures: A semiempirical approach. *Journal of Chemical Phsysics*, 114(15):6759–6762, APR 15 2001. ISSN 0021-9606.

[108] A. H. Taub. Relativistic fluid mechanics. *Annual Reviews in Fluid Mechanics*, 10(301–332), 1978.

[109] J. J. Thomson. On the analogy between the electromagnetic field and a fluid containing a large number of vortex filaments. *Phil. Mag. S.*, 12 (80):1057–1063, November 1931.

[110] José Trueba and Antonio F. Rañada. The electromagnetic helicity. *The European Journal of Physics*, 17:141–144, 1996.

[111] José Trueba and Antonio F. Rañada. Helicity in classical electrodynamics and its topological quantization. *Apeiron*, 7(1-2):83–88, January-April 2000.

[112] David Turnbull. Kinetics of solidification of supercooled liquid mercury droplets. *The Journal of Chemical Physics*, 20(3):411–424, 1952. doi: 10.1063/1.1700435.

[113] S. Webb, editor. *The Physics of Diagnostic Imaging Second Edition*. CRC Press (Institute of Physics Publishing(, 1988.

[114] J. H. Weijs, James R. T. Seddon, and D Lohse. Diffusive shielding stabilizes bulk nanobubble clusters. *ChemPhysChem*, 13:2197–2204, 2011.

[115] Wen-Yang Wen and John A. Muccitelli. Thermodynamics of some perfluorocarbon gases in water. *Journal of Solution Chemistry*, 8:225–246, 1979. ISSN 0095-9782. 10.1007/BF00648882.

[116] G. W. Willard. Ultrasonically induced cavitation in water: a step by step process. *The journal of the acoustical society of america*, 25(4):669–686, July 1953.

[117] Ludwig Wittgenstein. *Tractatus Logico-Philosophicus*. Routledge Classics, 2002, 1921. Translated by D.F. Pears and B.F. McGuinness.

[118] Boguslaw Wolniewicz. *Logic and metaphysics. Studies in Wittgenstein's ontology of facts*. Warsaw: Polskie Towarzystwo Semiotyczne, 1999.

[119] Zhanwen Xing, Jinrui Wang, Hengte Ke, Bo Zhao, Xiuli Yue, Zhifei Dai, and Jibin Liu. The fabrication of novel nanobubble ultrasound contrast agent for potential tumor imaging. *Nanotechnology*, 21(14):145607, 2010.

[120] Jonathan S. Yedidia. An idiosyncratic journey beyond mean field theory. In D. Saad and M. Opper, editors, *Advanced Mean Field Methods - Theory and Practice*. MIT Press, 2000.

[121] David E. Yount. Skins of varying permeability: A stabilization mechanism for gas cavitation nuclei. *The Journal of the Acoustical Society of America*, 65(6):1429–1439, 1979. doi: 10.1121/1.382930.

[122] H.R. Zheng, S. Mukdadi, and R. Shandas. Theoretical predictions of harmonic generation from submicron ultrasound contrast agents for nonlinear biomedical ultrasound imaging. *Physics in Medicine and Biology*, 51(3):557–573, Feb 2006.